CONF-760935--53

CONCEPTUAL DESIGN OF SUPERCONDUCTING MAGNET SYSTEMS FOR THE ARGONNE TOKAMAK EXPERIMENTAL POWER REACTOR

S. T. Wang, L. R. Turner, F. E. Mills,
D. W. DeMichele, P. Smelser,
and S. H. Kim

The Technology of Controlled Nuclear Fusion
American Nuclear Society
Richland, Washington
September 21-23, 1976

CONCEPTUAL DESIGN OF SUPERCONDUCTING MAGNET SYSTEMS FOR THE ARGONNE TOKAMAK EXPERIMENTAL POWER REACTOR *

S. T. Wang, L. R. Turner, F. E. Mills,
D. W. DeMichele, P. Smelser and S. H. Kim

CTR Program
Argonne National Laboratory
Argonne, Illinois 60439

As an integral effort in the Argonne Tokamak Experimental Power Reactor Conceptual Design,[1] the conceptual design of a 10-tesla, pure-tension superconducting toroidal-field (TF) coil system has been developed in sufficient detail to define a realistic design for the TF coil system that could be built based upon the current state of technology with minimum technological extrapolations. A conceptual design study on the superconducting ohmic-heating (OH) coils and the superconducting equilibrium-field (EF) coils were also completed. These conceptual designs are developed in sufficient detail with clear information on high current ac conductor design, cooling, venting provision, coil structural support and zero loss poloidal coil cryostat design. Also investigated is the EF penetration into the blanket and shield.

SUPERCONDUCTING TOROIDAL-FIELD COIL SYSTEM

Characteristics of Toroidal-Field Coil Design

The TF coil uses niobium-titanium as the superconductor because of its good ductility and proven performance in large magnets. The toroidal field strength should be as high as practical in order to enhance the plasma confinement and boost the power performance. A peak field of 10 T can be achieved with a large amount of superconductor at 4.2°K or with much less superconductor at 3°K. It is more economical to operate the 10 T TF coil at 3°K because the difference in refrigeration cost is much smaller than the difference in the cost of the superconductor. The problem of refrigeration at temperatures lower than 4.2°K for large systems was evaluated. The TF coils will achieve 10 T peak field at 3°K and 8 T peak field at 4.2°K with about 0.5°K temperature allowance for each case; 8 T is the minimum goal and 10 T is the maximum goal in the TF coil design.

A TF coil system consisting of 16 pure-tension "D"-shape coils with a horizontal bore of 7.78 m provides adequate space for the vacuum chamber, blanket and shield; provides adequate access for assembly and repair; and has a satisfactorily small maximum field ripple of 1.3%. The TF coil system is summarized in Table 1 and depicted schematically in Figure 1.

The hoop tension acting on a circular or oval toroidal coil system, either a continuous toroid or a bumpy toroid, is

* Work supported by the U. S. Energy Research & Development Administration.

TABLE 1. Toroidal Field Coil System

Number of coils	16
Coil shape	pure tension
Maximum access (m)	~ 3
Peak field (T)	
10	3°K
8	4.2°K
Bore (m)	
Vertical	12.6
Horizontal	7.78
Field in plasma, B_t (T)	
10 T peak field	4.32
8 T peak field	3.46
Operational current (kA/turn)	60
Stored energy (GJ)	30 total
Inductance (H)	16.7 total
Ampere-turns (MAT)	134 total
Turns/coil	70 x 2
Mean turn length (m)	36
Coil weight/coil (Ton)	~ 208
Coil and bobbin cross section (m^2)	0.619
Winding cross section (m^2)	0.572
Average current density (A/cm^2)	
Over bobbin and coil	1352
Over coil winding	1463
Over copper	3660
Average turn cross section (cm^2)	40.6
Cross section ratio, SS/Cu	~ 1.5
Refrigeration power (MW)	14.3

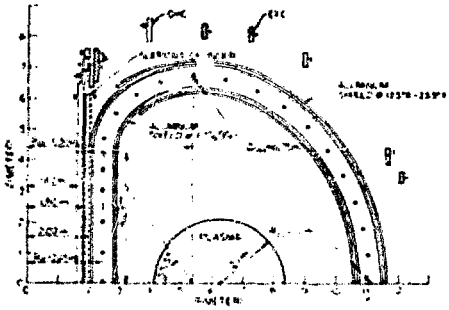

FIGURE 1. EPR Magnet Schematics

nonuniform. Large bending moments are exerted on the conductor. This produces high peak stresses; consequently, a larger amount of structural material will be needed than in the absence of bending moments. Although it is possible to contain the bending moment by an external mechanical structure, to do so may not avoid conductor slippage, and large shear stresses may exist from turn-to-turn and/or layer-to-layer. When the radius of curvature is such that the product of transverse force and radius of curvature is constant, the coil is in pure tension with no bending moments; then, a minimum amount of structural material will be needed and the in-plane hoop stress will be uniform with inner skin stress slightly higher than outer skin stress. The mean hoop stress will be the average value of the inner skin stress and the outer skin stress, as shown in Figure 2. Therefore, the toroidal coil system will behave exactly like a solenoid. The solenoid is known to the superconducting magnet engineer as the coil which is most stable and has the least mechanical disturbance. Consequently, it is expected that the coil stability of a pure-tension coil system will be better than that of circular or oval coil systems. For the 10-T TF coil design, the average hoop stress is about 21,000 psi.

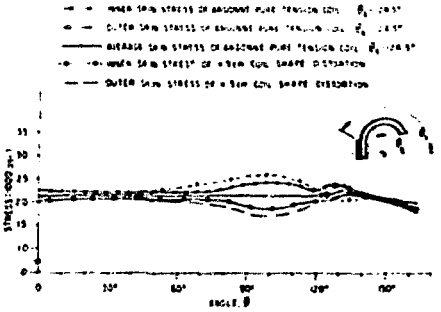

FIGURE 2. Hoop Stresses Distribution of Argonne Pure-Tension Coil.

Superimposing Fields and Out-of-Plane Loads

With a TF peak field of 10 T, the plasma current will be 7.6 MA. The ohmic-heating (OH) coil of ± 67 MA turns will swing a central field of ± 5 T. The equilibrium-field (EF) coil of 37.15 MA turns will generate 0.46 T at the plasma center for plasma equilibrium. Without a field shield, these poloidal coils and plasma currents would superimpose ac field onto the TF coil windings, exerting an out-of-plane load onto the TF coil, as well as producing large ac losses. The performance and design of the TF coil is severely affected by the superimposing fields. The OH coils produce little superimposing field, while the plasma current generates large amounts of parallel fields. The EF coil contributes large amounts of both parallel and perpendicular fields.

To compute the out-of-plane load exerted on the TF winding, the superimposing fields from the OH coils, the EF coils and the plasma were computed at various times in the cycle. The TF coils were divided into 70 angular segments with approximately equal angular spacings. On each angular segment cross section, superimposing fields were computed at nine locations. The out-of-plane load was obtained by Gaussian integration of the $\vec{J} \times \vec{B}$ body force over the superimposing fields at nine points. Computations at various times were necessary because the OH coils, the EF coils and the plasma contribute different amounts at different times. The distribution of out-of-plane loads at 5 representative times is shown in Figure 3(a), (b), (c), (d) and (e), respectively. It is important to note that there are many local bending moments exerted on the TF coil. (The out-of-plane load of the lower coil half is the mirror image

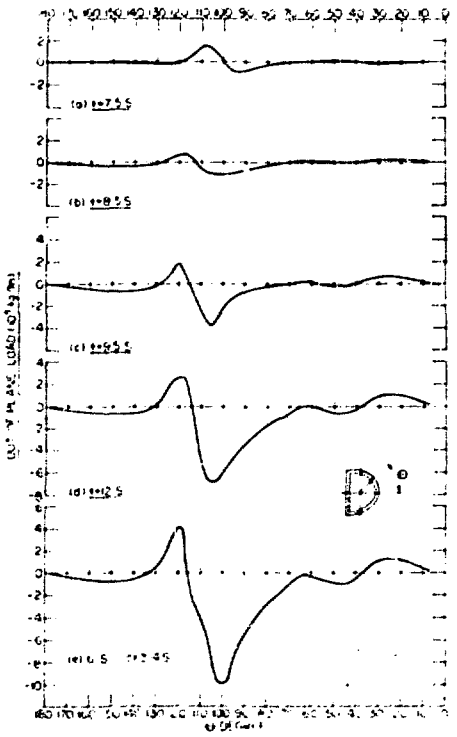

FIGURE 3. Time Evolution of Out-of-Plane Load.

of that for the upper coil half.) Surprisingly, the sign of the out-of-plane load reverses rapidly from segment to segment. For this EPR design, the most severe out-of-plane load acts on the coil segments within the angular position between 85° and 125°. The maximum out-of-plane load occurs during the burn phase with a maximum out-of-plane pressure of about 3000 psi at the 100° position. Since many bending moments exist along the TF coil, shear members will be effective for the out-of-plane load support.

Normal Metal Field Shielding Design

The TF coil reference design provides normal metal field shielding. With a field

shield, a monolithic conductor can be used without excessive ac losses. Without the shield, cable conductor must be used provided that all filaments in the cable are fully transposed. There is little experience of using cable conductor in a large magnet. It is fair to say that the sponginess of a cable conductor raises questions about its use in a large magnet system with large electromagnetic forces. As far as mechanical integrity is concerned, monolithic conductors are far better than cable conductors.

High-Purity Aluminum as Normal Metal Shield

High-purity aluminum or copper has a large residual resistivity ratio (RRR = $\rho_{273°K}/\rho_{4.2°K}$), on the order of 10^3 to 10^4. However, the large magnetoresistivity of copper severely reduces its conductivity gain at low temperatures. Aluminum, on the other hand, has a rather small magnetoresistivity that saturates at a rather low field ($\sim$ 0.5 T). The low magnetoresistivity of aluminum recommends it for use as the normal metal shield. To keep the strain-induced resistivity small, the aluminum must be reinforced. For example, if aluminum is explosively welded to stainless steel, then the stainless steel will be stressed to 60,000 psi while the aluminum suffers a strain of only 0.17%. The 0.17% strain cuases little increase in resistivity. For 5000 purity aluminum reinforced by stainless steel, recent data indicate that there is little increase in resistivity for up to 300 loading cycles.[2]

The 5000 purity aluminum with stainless steel backing is chosen for the field shield panels. These panels are formed into rectangular ducts around the TF coil as shown in Figure 1. For the present design, the shields around the inner leg of the TF coil are seriously restricted by the available space and are, therefore, wrapped directly on the TF coil form. The operating temperature is 3°K or 4.2°K depending upon the 10 T or 8 T operation. The remaining shields will be operated between 12.5°K and 23.5°K with a mean temperature of 18°K. Shield panels inside the TF coil will be subjected to a peak field ranging from 3 T to 10 T. The side panels will have an averaged magnetic field ranging from 1.5 T to 5 T. The outside panels will be subjected to only the ac superimposing field of 0.5 T. The overall averaged magnetic field in the shield is about 4 T. The resistivity[1] of 5000 purity aluminum at 3°K or 4.2°K and 4 T field is about 2 x 10^{-11} Ω-m.[1] These data are based on transverse magnetoresistivity measurements. The longitudinal magnetoresistivity, in general, is slightly smaller than the transverse values for the same purity of aluminum. At 18°K and 4 T field, the penetration depth for the 5000 purity aluminum is 3.1 cm for a period equal to 75 s. At 3 to 4.2°K and 4 T field, the penetration depth is about 1.95 cm. To provide nearly complete shielding, the 18°K shield should have a thickness of 5 cm. The 3 to 4.2°K shield should have a thickness of 4 cm.

AC Losses in Aluminum Shield

The reference cycles for the EF coil, the OH coil and the plasma current are shown in Figure 11. The ac losses in the field shield can be separated into those due to perpendicular fields and those due to parallel fields.

For a change of magnetic flux parallel to the TF coil, we can treat the shield as a long solenoid, with uniform induced flux within. The induced voltage, $\dot{\phi}_{App}$, from a

sinusoidal time variation of the applied flux can be written as

$$\dot{\phi}_{App} = j\omega B_0 A \exp(j\omega t) = L\ell\, \dot{I}/\ell + R\ell\, I/\ell.$$

Here the length, ℓ, of the shield has resistance, R, and inductance, L, given approximately by

$$R\ell = \rho p/X,$$

$$L\ell = \gamma \mu_0 A,$$

where p and A are, respectively, the cross sectional perimeter and enclosed area of the shield, ρ is the electrical resistivity, $\mu_0 = 4\pi \times 10^{-7}$ H/m. The current depth, X, is determined by the smallest of three lengths: the shield thickness t, the skin depth δ, and the so-called mean hydraulic depth A/p. Then, the average power dissipated per unit length is

$$\frac{\bar{P}_{II}}{\ell} = \frac{X\,\omega^2 B_0^2 A^2}{2\,\rho p\,[1 + (\gamma\omega\mu_0\, AX/\rho p)^2]} .$$

In the limit of low conductivity ($R \gg \omega L$), the above equation becomes

$$\bar{P}_{II}/\ell = X\,\omega^2 B_0^2 A^2/2\rho p ,$$

and in the high conductivity limit ($R \ll \omega L$), it becomes

$$\bar{P}_{II}/\ell = \rho p B_0^2/2\ X\ \gamma^2 \mu_0^2 . \qquad (1)$$

If the time-varying field is perpendicular to the axis of the shield, the general eddy-current problem does not have an analytic solution. For a circular cross section shield of radius a in the high conductivity limit with $\gamma = 1$, the power is given by

$$P_\perp/\ell = 4\pi a B_0^2 \rho/2\ X\mu_0 = \rho p B_0^2/X\mu_0^2 = 2\,(\bar{P}_{II}/\ell) . \qquad (2)$$

From Equations 1 and 2 we can obtain the power loss in the shield of a TF coil in a sinusoidally-varying flux, if the high-conductivity limit applies

$$\bar{P} = (\rho p/X\mu_0^2) \oint (B_{0\perp}^2 + 1/2\ B_{0II}^2)\, d\ell . \qquad (3)$$

If the time variation is not sinusoidal, but given by the Fourier series,

$$B(t) = B_0 \sum_{n=0}^{\infty} a_n \cos 2\pi nt/\tau ,$$

with τ the period, and if $X = \delta_n = (2\rho/\mu_0\omega_n)^{1/2} = \sqrt{n}\,\delta_1$, then Equation 3 becomes

$$\bar{P} = (\rho p/\delta_1 \mu_0^2) \oint (B_{0\perp}^2 + 1/2\ B_{0II}^2)\, d\ell \sum_{n=1}^{\infty} \sqrt{n}\, a_n^2 . \qquad (4)$$

Since the three poloidal field wave forms are not alike, each individual wave form is expanded into a Fourier cosine series with coefficients evaluated separately. The Fourier series representing the resultant superimposing field is equal to the sum of the three individual Fourier series.

The ac loss distributions,[1] expressed as the power dissipation per meter, are shown in Figure 4. The total ac losses for the 3°K shield are 298.6 W per TF coil, with 147 W as the perpendicular field dissipation and 151.6 W from the parallel field loss. The remaining shields will be refrigerated between 12.5°K and 23.5°K with a mean temperature of 18°K. The shields will be bonded to a stainless steel backing of 1 cm in thickness. The total ac losses of the 18°K shield is 8.531 kW per coil with 3.295 kW from parallel field and 5.236 kW from perpendicular field losses.

DC Field Soaking

About 70% of the superimposing field is the dc field component. The dc field will soak through the aluminum shield in a time

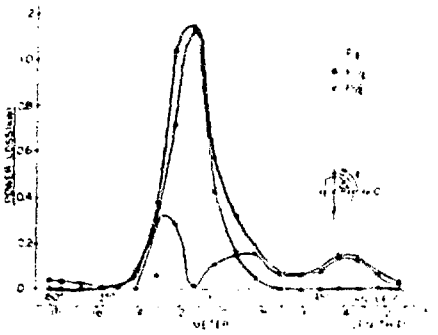

FIGURE 4. AC Losses Distribution Along the TF Coil.

constant of 6 minutes. The 6 minutes soaking time constant is considered rather long compared with the current ramping time of 2 s. Once soak through is complete, the dc field will remain as a static field interacting with the TF coil current producing 70% of the out-of-plane load previously calculated.

Out-of-Plane Load in Shield

The aluminum shield is now subject to the cyclic out-of-plane loads. If the superimposing fields had a time dependence that was a pure sine wave with no dc component, then the out-of-plane load on the shield would be the same as it would be on the TF coil in the absence of the shield. The loads on the shield are now due to the forces exerted by the toroidal field on the eddy currents in the shield. The distribution of the out-of-plane load on the shield is very similar to that in Figure 3(e) (load on TF coil with no shield) but at only 30% of the magnitude. There are, in addition, in-plane forces and twisting moments. Their magnitudes are such that their support appears manageable.

Conductor Design and Coil Structure

The full stability of the conductor will be assured if the conductor has good mechanical stability in a proposed coil structure. Careful investigation on all the forces exerted on the TF coil conductor reveals that there are at least four significant mechanical instabilities in a TF coil. These are as follows: (1) Out-of-Plane Load - Both the local moments and the over-turning moments are quite capable of generating shear stress between turns or between layers; (2) The Centering Force - Conductors, insulators and structural materials in the TF straight segment at the inner leg will experience a large radial inward compression of about 8000 psi. This will likely generate layer-to-layer shear unless each layer is flat and firm enough to support its neighboring layer; (3) Gravitational Load - The fact that the TF conductor in each coil weighs about 208 tons and is standing in a vertical plane could cause a problem in mechanical instability; (4) Other Bending Moments - Bending moments of a pure-tension TF coil may still exist if the coil shape is distorted because of imperfection in coil winding and the deflection of conductor and coil form due to g-load. Bending moments may also be developed if there is an in-plane coil displacement due to the imperfection of coil fabrication and assembly.

Based on the preceding design considerations, it is proposed that a wide sheet conductor, as shown in Figure 5, be used in the TF coil if a field shield is provided.

With two subdivisions in each TF coil and one turn per layer in each subdivision, the conductor stabilizer width will vary from $\sim$ 0.5 m for the innermost layer to 0.3 m for the outermost layer. Reasonable thickness per layer is needed to increase the out-of-plane rigidity and to avoid troubles in handling wide and thin metal sheet. A

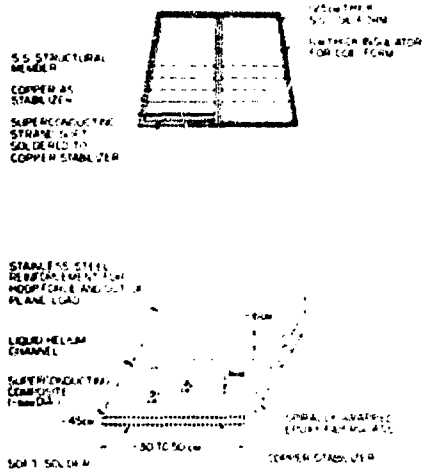

FIGURE 5. Reference Sheet Conductor (60 KA) for TF Coil and its Coil Cross Section (Jelly Roll Winding).

current of 60 kA per turn was tentatively determined; typical dimensions for copper sheet, stainless steel reinforced sheet and the proper superconductor cross section in each field region were chosen. The superconductor cross section was sized using a J-H curve with a temperature 0.5°K above the intended operating temperature. The conductor is graded into nine field grades between 3 T and 10 T. This is because the outermost layer conductor in the outer TF leg will see a field of 3 T rather than zero. Substantial cost saving can be made if conductor is graded in this manner.

The proposed sheet conductor is made of a copper sheet and many superconducting composite wires stranded around it. This stranding is necessary to eliminate the self-field instability that will be significant if the operational current is large. To assure good bonding, the strands are soft-soldered to the copper sheet.

The fiberglass epoxy is spiral wrapped around the sheet conductor covering 50% of the exposed surface. This will provide an exposed surface area of about 50 cm^2 per cm conductor length. The equivalent recovery heat flux per cm^2 is about 0.3 W. The coil form is stainless steel and insulated with a micarta or G-10 sheet of 1 cm thickness. These sheets are grooved to provide vertical liquid helium channels for venting.

A stainless steel sheet of variable thickness is wrapped along the conductor. As far as hoop stress is concerned, the multilayer stainless steel serves as a multishell stainless steel pressure vessel. For the out-of-plane load, the stainless steel sheet increases the rigidity of the coil form tremendously. Since the radius of curvature near a 10 T region is 1.98 m, the overall average hoop stress in stainless steel is 26,000 psi and that in copper stabilizer is 14,500 psi. These stress levels are fairly conservative at 4.2°K temperature.

Summation of Dissipation Loss and the Refrigeration Requirements

Heat dissipation in the TF coil system is summarized in Table 2. A neutron wall load of 0.5 MW/m^2 is used to compute the nuclear heating for both the 8 T and 10 T operation. As to the cryostat loss, the radiation loss between the 18°K field shield and the 3°K helium vessel is negligibly small. The radiation heat load from the 300°K vacuum wall to the 18°K shield is 64.5 W per TF coil or 1032 W for all 16 coils provided that multiple layer superinsulation is used. The heat conduction loss through the support system is small and there is no loss for the intercoil structure. The 60 kA leads will dissipate a total of 120 W.

Therefore, the total loss in the 3°K helium vessel is 6.40 kW for all 16 coils. The total loss in the 18°K normal metal shield is 137.5 kW for all 16 coils. If the TF coil is operated at 8 T, then the coils will be at 4.2°K. The ac loss in the 4.2°K helium vessel will be reduced by a factor of 0.64 relative to the 3°K use. The ac loss in the 18°K aluminum shield will also be reduced by a factor of 0.64. This is because the ac loss mainly is produced by the EF coil and the plasma current. Therefore, at 8 T operation, the total losses in the 18°K normal metal shield are 88 kW for all 16 coils. These losses, as well as the ac losses without field, are tabulated in Table 2.

The Effects of Fabrication Tolerances

The effects of TF coil fabrication tolerances include the imperfection of coil winding, the tolerances of coil forms, the static g-load deflection, the error in the assembly and the possible errors due to thermal contraction. Fabrication tolerance has been studied in five categories as follows (see Figure 6): (1) The TF coil shape may be distorted uniformly above or below the pure-tension shape by 5 cm; (2) The TF winding may be displaced radially or vertically by about 2 cm during assembly or cooldown; (3) The TF coil may be rotated by about 0.5° in the toroidal direction during the winding, cooldown or assembly; (4) The TF coil may be tilted about the

TABLE 2. TF Coil Heat Dissipation Summary

Heat Dissipation Item	With Aluminum Field Shield (Sheet Conductor)				Without Field Shield* (Cable Conductor — Pure Tension Reference)			
	10 T (3°K)		8 T (4.2°K)		10 T (3°K)		8 T (4.2°K)	
	Per Coil (W)	16 Coils (kW)	Per Coil (W)	16 Coils (kW)	Per Coil (W)	16 Coils (kW)	Per Coil (W)	16 Coils (kW)
Nuclear Heating	91	1.5	91	1.5	91	1.5	91	1.5
3°K/4.2°K Al. Shield ac Losses	299	4.8	191	3.06	--	--		--
18°K Al. Shield ac Losses	8500	136	5500	88	--	--	--	--
Thermal Radiation Load on 18°K Shield	65	1.04	65	1.04	--	--	--	--
Thermal Radiation Load on Helium Vessel from 77°K shield	--	--	--	--	10	0.16	10	0.16
Structal Heat Conduction Loss on Helium Vessel	10	0.16	10	0.16	10	0.16	10	0.16
Current Leads Loss	--	0.32	--	0.32	--	--	--	--
Parallel Field Conductor Loss**	--	--	--	--	906	5.74	337	5.39
Perpendicular Field Conductor Loss**	--	--	--	--	130	2.08	85	1.35
AC Loss in Coil Form	--	--	--	--	641	10.3	401	6.46
Summation of Loss at 3°K/4°K	400	6.4	300	4.8	1544	24.7	970	15.5
Summation of Loss at 18°K	8565	137	5565	89	--	--	--	--
Refrigeration Power (Compressor Input power)	16.1 MW		8.9 MW		9.1 MW*		6.7 MW*	

* AC Loss in Conductor reinforcing structural material is not included.

** Because of complex nature of $\dot{B}$ in the plasma ramping and TF Coil ramping, 2 s rise time is used in this calculation. The conductor is a hypothetical conductor used in the ac losses calculation.

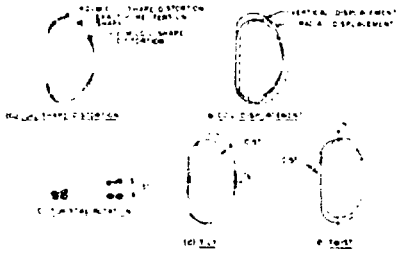

FIGURE 6. Five Possible Fabrication Tolerances.

horizontal axis by 0.5°; (5) The TF coil may be twisted about the vertical axis by 0.5°. It is clear that the effects of the first two fabrication errors will alter the transverse force pattern and induce bending moments in the otherwise pure-tension TF coil. To simulate the error in category (1), the pure-tension coil evolution was intentionally interrupted so that the coil shape is approximately 5 cm from the final pure-tension shape. The hoop stress analysis is shown in Figure 2. The coil displacement is done for one coil only. The result of these errors induce nonuniform hoop tension as shown in Figure 7.

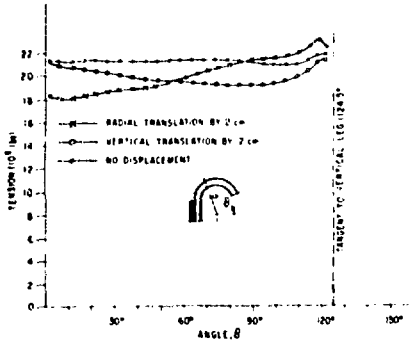

FIGURE 7. Tension Distortion of Coil Displacement and Coil Shape Deflection.

If the fabrication error falls into the third, fourth and fifth categories, the dominant effect is the unbalanced intercoil force in the toroidal direction as shown in Figure 8. It is seen that tilting and twisting by 0.5° will generate an additional attractive force on the order of 1 x 10^5 kg/m while a rotation of 0.5° produces an intercoil force of 4 x 10^5 kg/m.

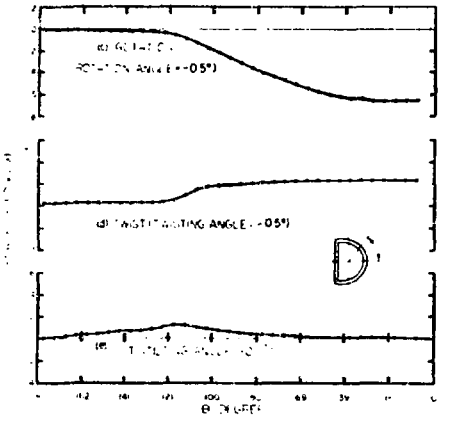

FIGURE 8. Out-of-Plane Load Due to Errors of Rotation, Twist and Tilt.

Coil Protection and Magnet Safety Analysis

Energy Release

The stored energy is 30 GJ in 16 coils at 10 T. The operational current is 60 kA and the total inductance is 16.7 H. This operational current is too large to allow one pair of leads out from each TF coil. Instead, only two leads, one from the number 1 TF coil and the other from the number 16 TF coil, are allowed to feed through the cryostat. All other connections between adjacent coils are done through intercoil tubing connecting the two adjacent cryostats. Therefore, for this design, the energy dumping circuit is shown in Figure 9. The dump resistor must always be connected to

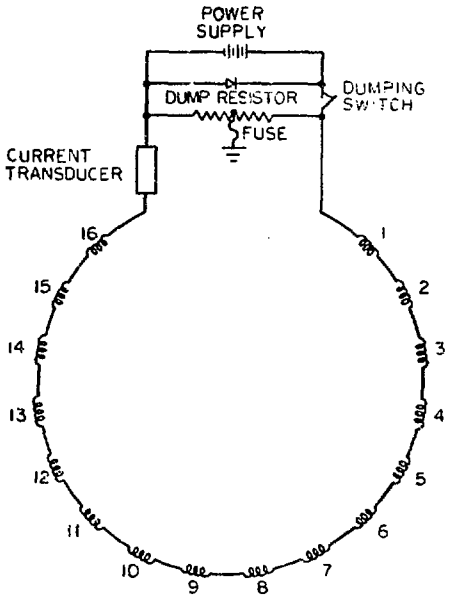

FIGURE 9. Dumping Circuit

the coil. The coil system energy will be discharged through the dump resistor. The terminal voltage of the magnet will be no greater than the voltage across the dump resistor. The discharge voltage will be 2000 V. The resistance of the dump resistor will be 0.033 Ω and the coil current will decay in a time constant of 506 s, or 8-1/2 minutes.

As shown in Figure 9, a fuse with a small current capacity is connected in the grounding loop to the discharge resistor to ensure that no large grounding current shall flow if any point in the coil winding should accidently be grounded. The discharge resistor must be tested at incrementally increasing current levels during initial system checkout. Multiple parallel paths should be provided in case interruption may occur in the discharge resistor.

Arcing

Arcing is always a serious threat to a large superconducting magnet, a large safety margin must be used in designing the coil insulation and the current leads insulation. For example, the 4000 V coil insulation must be provided in order to allow a 2000 V operating condition. In fact, the entire system should be tested with a high voltage and extreme low current output power supply to test the insulation strength of the coil with respect to ground under the liquid helium environment.

Coil Forces and Structure Stress

The most critical hazards are those in which the design forces in the conductor and forces in supporting structures are exceeded. Therefore, strain gauges are used to monitor these situations.

Cryostat Protection

Each TF coil cryostat shall be equipped with pressure rupture discs to guard against pressure buildup in the helium vessel.. The pressure rupture disc can also protect the magnet coil in the event that large resistive heating occurs with rapid pressure rise. Then, at a preset pressure, the rupture disc breaks and the bulk of the liquid helium will be rapidly transferred from the dewar to an emergency dump tank. This will remove liquid helium quickly and the whole coil will become normal and coil energy will be uniformly dissipated throughout the winding.

Short

Shorting from turn-to-turn, from layer-to-layer or from coil-to-ground is a very serious matter. The short will act as a discharge resistor. Should the coil energy be discharged, large amounts of energy deposition will occur at the short, and the conductor around the short will be melted into a copper block. Techniques for testing

the short must be developed. Potential taps for checking shorts after the coil is wound must be incorporated.

Current Leads Protection

If the discharge time constant is 8-1/2 minutes, then the current leads must be designed to allow adiabatic heating in that time period without raising the lead temperature dangerously high. The current leads are cooled by counter-flow helium gas. In-line gas flowmeters must be installed to monitor the amount of counter-flow helium gas. Alternatively, voltage taps across the leads are provided to monitor the current lead temperature. Temperature sensors may also be attached to the connector of the current leads.

Current leads are a weak link in magnet systems. The magnetic field and forces on the lead must be carefully evaluated. The leads must be firmly supported and must have sufficient insulation.

Connectors and Conductor Joints

Connectors and conductor joints are another weak link in the magnet system. The resistance of each joint and each connector must be carefully tested and voltage taps must be provided across the joints and connectors to monitor possible failures. All forces exerted on the connectors and joints must be carefully computed. The mechanical strength of joints and connectors must be thoroughly tested. In some instances, a redundant path should be provided.

Bending Moments

When two neighboring coils carry different currents, the unbalanced intercoil force is large. Furthermore, pure-tension TF coils will remain in pure tension only if all coils carry the same currents. If two coils carry different currents, large bending moments and peak stresses will occur in the coil and subsequent structure failure may occur. Therefore, it is exceedingly important to make sure the currents are the same. This probably can be guaranteed only through series operation under all circumstances.

Eddy Current Interaction

If the magnet is discharged in 8-1/2 minutes, large eddy currents will be developed in each vacuum vessel and the field shield. The interaction between the eddy currents and the decaying field may generate a large and complex force and ruin the field shield or radiation shields or structural members.

SUPERCONDUCTING POLOIDAL COIL SYSTEMS

Poloidal Field Coil Characteristics

The poloidal field coils consist of the OH coils and the EF coils. The OH coils and the EF coils are superconducting and are located outside the TF coils, as shown in Figure 10.

Although the OH coils serve as the transformer primary for producing the plasma current and the EF coils provide equilibrium for the plasma, both coil systems have nearly identical problems, e.g. large stored energy, high operational current, rapid charging and discharging, and ring coil configuration. For this reason, the conceptual design of the eight pairs of EF coils (coil numbers 1 to 8) and six pairs of OH coils (coil numbers 9 to 14) were carried out together.

The design requirements for the OH and EF coil systems were specified as a result of a detailed trade-off study. Burn cycle dynamic simulations of the plasma, the coupled OH and EF systems, and the plasma heating systems were performed. Free-boundary plasma MHD equilibrium calculations[2] were utilized in the design of an equilibrium field that would produce the

TABLE 3. OH Coil/EF Coil Magnet Characteristics

	OH Coil	EF Coil
Superconductor/Stabilizer	Nb-Ti/Cu	
Coil design	Single layer	
Conductor design	Fully-transposed cable	
Stability	Cryostatic	
Cooling	Pool boiling	
Operating temperature (°K)	4.2	
Average current density (A/cm^2)	2640	2946
Magnetic field (T)		
in flux core	∿ 5	
at plasma center		∿ 0.46
Ampere-turns (MAT)	67	± 18.6
Total conductor length (MA meters)	847	996
Maximum dB/dt in conductor (T/s)	6.7	∿ 1
Stored energy in OH/EF/plasma field (MJ)	2262	
Maximum operational current (kA)	80	80
Number of turns	837	464
Self inductance (H)	0.48	0.52
Mutual couplings	$K_{OHEF} = 0.015$	
Power supply voltage (kV)	48	21
Volt-seconds to plasma (V-s)	85	50
Coupling coefficient to plasma ring	$K_{OHP} = -0.2422$	$K_{EFP} = -0.2566$

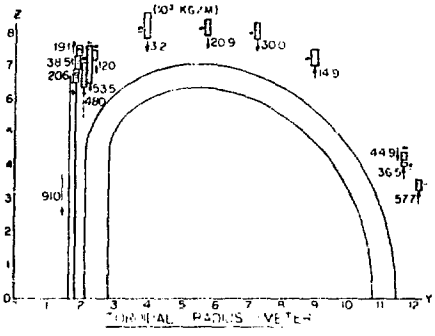

FIGURE 10. Vertical Force per Length During Burn Phase.

circular plasma. Characteristics of the OH and EF coils are given in Table 3.

The Superconducting OH/EF Coil Design

The poloidal coil design calculations were based on a design-basis burn cycle as shown in Figure 11.

The total volt-second requirement for the reference design is 135. The OH coils are capable of reversing from -5 T to +5 T, supply 85 V-s, with an OH flux core radius of 1.7 m. The EF coil will supply the remaining 50 V-s.

The OH coils are located outside the TF coil system so that the winding can be arranged to minimize the ac superimposing

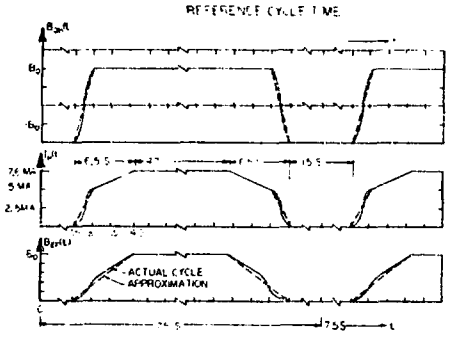

FIGURE 11. Reference Cycles for OH Coils, EF Coils and Plasma.

field on the TF coil. Since the OH coil is at full negative value before the onset of plasma startup, the OH coil windings must also be distributed so that the field produced by the OH coils at the plasma are less than 10 G or so. This requirement must be fulfilled in order to guarantee a stable startup. With these considerations in mind, the OH coils are arranged as shown in Figure 10. The winding dimensions are shown in Table 4, where R_1, R_2, Z_1 and Z_2 represent the inner radius, the outer radius, the initial axial coordinates and the final axial coordinates, respectively.

If the EF coils were placed inside the TF coils, there would be tremendous difficulties in coil assembly, disassembly, support, repair and maintenance, as well as in the assembly, disassembly and maintenance of the blanket and shield and the first wall. To avoid these problems, the EF coils are located outside the TF coils.

The OH coils would induce large voltages in the EF coils, if the EF coils were not decoupled from the OH coils. The decoupling ampere-turns should be positioned so that they produce small anti-vertical fields and small superimposing fields on the TF coils.

Axial Forces, Hopp Stress and Coil Interaction

In the EPR poloidal coil system, since all of the fourteen poloidal coils and the plasma ring contribute to the magnet field at any poloidal coil winding, the axial force and pressure of each coil depends on

TABLE 4. Poloidal Coil Winding Configurations

Coil Number	Z_1 (m)	Z_2 (m)	R_1 (m)	R_2 (m)	Coil Pair NI (MAT)	Coil Pair Cond. Lgth. (40 kA-m)
1	3.25	3.584	12.0	12.15	2.95	5599
2	4.15	4.417	11.55	11.70	2.36	4309
3	7.0	7.50	8.85	9.0	4.42	6195
4	7.8	8.30	7.10	7.25	4.42	4980
5	7.90	8.40	5.60	5.75	4.42	3939
6	7.16	7.44	2.25	2.40	- 2.48	904
7	6.48	7.571	2.10	2.25	- 9.642	3294
8	6.35	7.081	1.95	2.10	- 6.46	2055
9	0	6.5	1.62	1.77	51.48	13707
10	6.50	5.9	1.70	1.85	3.17	883
11	6.90	7.3	1.75	1.90	3.17	908
12	7.30	7.6	1.80	1.95	2.38	700
13	7.80	8.6	3.80	3.95	6.34	3857
14	4.03	4.1	11.55	11.70	0.55	1012

excitation of all coils. Therefore, it is difficult to predict either the magnitude or the direction of the vertical forces. It is entirely possible that during complete cycle the direction of vertical force at any coil reverses and that the magnitude of the vertical force changes rapidly in disproportion to self-excitation of that coil. Figure 10 shows the vertical force per meter coil length during the burn cycle with 7.58 MA plasma current, 5 T central field in OH coils and full excitation in EF coils. Note that some coils are subjected to repulsive forces while other coils are subjected to attractive forces. Note that some adjacent ring coils are subjected to vertical forces with opposite direction.

To obtain full information on vertical forces, the vertical forces on each coil were computed at different times during the entire reference cycle. The results are shown in Figure 12. Also investigated are the vertical forces on each coil when the plasma current suddenly quenches, a highly probable case for an EPR. It is interesting to note that, for all cases investigated, the vertical forces for coil numbers 2, 3, 4, 5, 6, 7, 11 and 13 will reverse their directions and coil supports for these coils must provide support in both directions.

The vertical force on the long solenoid is a body force and little structural support is needed. The vertical forces on coil numbers 6, 7, 8, 10, 11 and 12 will be transferred to the TF coil support cylinder with restraining rings for repulsive forces. Fortunately the remaining poloidal coils (namely, coil numbers 1, 2, 3, 4, 5, 13 and 14) have rather weak forces (no greater than 83×10^3 kg/m).

Although axial compressive stress for an ordinary solenoid is generally small in comparison with hoop stress, the axial pressure on the poloidal coils may be quite high because these axial forces result from many coil interactions. Computations of axial compressive pressure distributions for four typical poloidal coils are shown in Figure 13. It is seen that most poloidal coils have small compressive pressures (less than $\sim$ 100 kG/cm^2 or 1423 psi) with the exception of coil numbers 7, 8 and 9. The maximum compressive stress in coil numbers 7, 8 and 9 are 240 kg/cm^2, 301 kg/cm^2 and 592 kg/cm^2, respectively. These do not present mechanical problems.

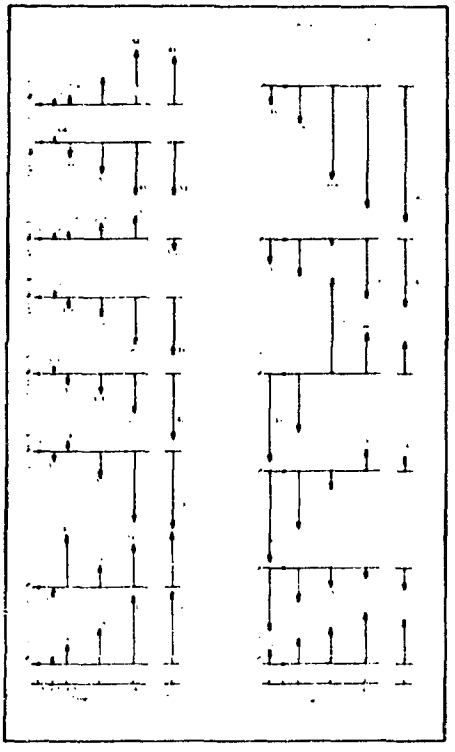

FIGURE 12. Axial Force per Unit Coil Length (10^3 kg/m).

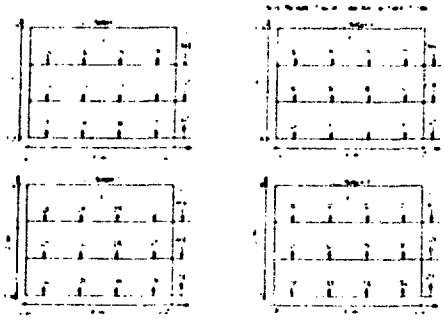

FIGURE 13. Axial Pressure, P (kg/cm^2), and Vertical Force, F (tons).

Computation of hoop stresses in a multilayer solenoid is a complicated problem because the hoop forces on any given turn will depend not only on the jRB_z of that turn but also on the interaction body forces resulting from the other turns pushing on it. The exact solution is further complicated by the inhomogenous coil structure. Since the proposed poloidal coils in the EPR will have one layer to avoid the high voltage insulation problem, the hoop stress in any given turn is independent of all other turns. The average hoop stress is given by

$$\bar{\tau}_r = j_{avg} \bar{R} \bar{B}_z,$$

where $\bar{R}$ is the mean radius of the turn and $\bar{B}_z$ is the axial field component averaged over the turn cross section.

The averaged hoop pressure or magnetic pressure, assuming no body force interaction from neighboring turns among successive layers, can easily be shown to be

$$\bar{\tau} = j_{avg} t \bar{B}_z,$$

where t is the radial thickness of the turn.

The computed $\bar{\tau}_t$ and $\bar{\tau}_r$ for the poloidal coils are tabulated in Table 5. It is interesting to see that coil numbers 6, 7, 10, 11 and 12 have hoop compression rather than hoop tension. Also note that coil numbers 5, 6, 8, 13 and 14 have high-averaged hoop stress and must have a substantial amount of reinforcement materials in the winding. The radial magnetic pressures for all coils are not high and they present no problems at all.

Conductor Design and Coil Structure

The operational current for both the OH coils and EF coils is 80 kA, supplied by two parallel 40 kA cables with fully transposed strands. The OH coils will have 837 turns in each parallel path. The OH coils will be cycled by a homopolar generator with peak voltage of 48 kV across the OH coil terminals if the OH coils are charged from -5 T to +5 T in 2 s. The EF coils will have 464 turns in each parallel path. The charging voltage will be around 21 kV across the EF coil terminals. Hence, turn-to-turn voltage will be about 60 V for the OH coil and about 50 V for the EF coil. The breakdown electric field in a helium gas environment is about 200 V/mm. Therefore, minimum separation between two adjacent turns in the same layer is about 0.3 mm for the OH coils and 0.25 mm for the EF coils.

It is clear that multilayer coils will require large gaps between layers. This presents an awkward problem for coil design. It is especially true for the long coils such as the long solenoid of the OH coils. Although good dielectric materials such as G-10 fiberglass may be used to fill the gaps between layers, the magnet designer will still face problems because it is very likely that pinholes or cracks may exist in these materials when the magnet is energized. Therefore, the proposed OH coils and EF coils will be wound with a single layer conductor. The width of the

TABLE 5. Hoop Stress and Radial Pressure of Poloidal Coils During Burn Phase

Coil Number	j (A/cm²)	t (m)	$\bar{R}$ (m)	$\bar{B}_z$ (T)	$\bar{\sigma}_t$ (kpsi)	$\bar{\sigma}_r$ (kpsi)
1	2946	0.15	12.07	0.012	0.62	0.007
2	2946	0.15	11.63	0.29	14.3	0.19
3	2946	0.15	8.93	0.13	4.9	0.08
4	2946	0.15	7.18	0.39	12.0	0.25
5	2946	0.15	5.68	0.83	19.8	0.53
6	-2946	0.15	2.33	2.32	-22.8	-1.48
7	-2946	0.15	2.18	0.12	- 1.13	-0.08
8	-2946	0.15	2.03	-2.83	24.1	1.81
9	2640	0.15	1.70	1.41	9.1	0.8
10	2640	0.15	1.78	-2.11	-14.2	-1.2
11	2640	0.15	1.83	-1.20	- 8.2	-0.68
12	2640	0.15	1.88	-1.24	- 8.8	-0.71
13	2640	0.15	3.88	1.38	20.3	0.79
14	2640	0.15	11.63	0.37	16.7	0.21

conductor is 15 cm. Based on the information of axial compressive stress, this width will be adequate.

The EF coils and OH coils will be cooled by pool boiling at 4.2°K and 1 atm pressure. Pool boiling is simple, inexpensive, reliable and easy to control. Above all, since a rather small heat transfer flux is adequate to remove the conductor ac losses, the heat transfer flux ceases to be an important factor in determining the coil stability. The coil stability will depend on the conductor and the extent of coil disturbances. However, it is important to recognize that pool boiling will work for an ac magnet only if the helium bubbles, which are generated at a constant rate, can be properly vented to avoid bubble accumulation within the winding. This requirement further justifies the decision for a single-layer coil.

The 40 kA cable can be achieved by cabling a basic strand of 0.3 mm diameter as shown in Figure 14. In the basic strand

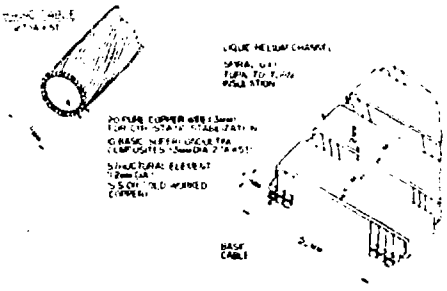

FIGURE 14. 40 kA Cable for Poloidal Coils

component, the copper to NbTi superconductor ratio is 2 to 1, with the NbTi cross-sectional area of 2.3×10^{-4} cm², or 1171 filaments with 5 m filament diameter. For a poloidal coil with a 5 T peak field, the conservative value of NbTi critical current density is about 117 kA/cm². Therefore, the basic strand shall carry 27 A. As shown in Figure 14, to assure current sharing with a higher Cu/NbTi ratio, 20

pure copper wires of 0.3 mm diameter were transposed along the 10 composite strands. High resistivity soft solder is used to solder these wires together around a central structural-reinforcing element. This raises the overall Cu/NbTi ratio of the basic cable to 11 to 1. This design offers good coil stability with low ac losses in mind. The composite with a single-component stabilizer rather than a cupronickel and Cu two-component stabilizer was chosen because of the rather poor conductor stability if cupronickel is incorporated. Therefore, as long as the ac loss is not too great, a conductor with a single-component stabilizer will be preferred. The basic cable shall carry 270 A at 5 T.

The 40 kA cable was finally achieved by transposing 150 basic cables into a height of 2 basic cables ($\sim$ 4 mm) by a width of 75 basic cables ($\sim$ 150 mm). The basic cable must be insulated with nomex paper before transposition. Otherwise, very large coupling eddy currents and ac losses will arise in the wide cable. Since the stability of the 40 kA cable is built into the stability of the basic cable, the fact that the basic cable is insulated probably will have no great effect on the stability of the 40 kA cable.

Finally, the 150 basic cables are banded together with spiral wrapping wetted fiberglass of 2 mm in thickness.

As shown in Figure 15, the poloidal coil is wound with a single layer wide cable of 40 kA.

The spiral wrapping fiberglass of 2 mm inch thickness will provide a turn-to-turn separation of at least 4 mm for adequate insulator. The width of the fiberglass is 2 cm and the wrapping pitch is 3 cm so that the liquid helium channel of 1 cm wide by

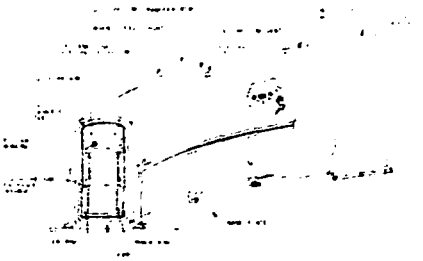

FIGURE 15. Poloidal Coil Structure and its Cryostat Configuration.

0.2 cm deep by 15 cm long will be provided on both faces of the cable. The bottom supporting plate is machined to have an inclined surface in the radial direction so that gas venting will move radially outward. An 0.1 mm nomex paper is used between turns to prevent the bubbles from rising through the turns. These measures should provide good bubble venting, separate the gas-liquid flow and allow each turn to see only the bubbles generated by itself.

The wrapped fiberglass is expected to be strong enough to transfer the hoop tension to the external rings, which are made to assist the hoop tension of the cable. The inner rings are made to overcome the hoop compression as well as to serve as the bobbin for winding. Many 2 mm wide slits are cut in these rings to allow gas venting and liquid circulation.

The axial compressive or repulsive forces of every 10 to 15 turns are supported by a 2-cm thick G-10 or micarta plate. This arrangement shall reduce the accumulation of axial compressive or repulsive pressures exerting onto the cable, which otherwise might short out the basic cables and deteriorate the coil stability.

Poloidal Coil Cryostat Design

Figure 15 illustrates a cryostat configuration for a poloidal coil. To reduce eddy current losses to a minimum, an essentially non-conductive inner shell is required. The illustrated design uses glass-reinforced epoxy, with an 0.013 cm layer of stainless steel for a helium permeation barrier. The construction technique consists of fabricating the shell by filament winding or braiding around the coil. The stainless steel barrier is installed after enough layers are built up to support it. Then fabrication continues until the required thickness is obtained.

The cryostat is insulated with high vacuum, plus a liquid-nitrogen-cooled radiation shield of laminated construction to minimize eddy current heating in the nitrogen shield. Multilayer insulation is used between the outer vacuum jacket and the nitrogen shield. The multilayer insulation is installed with the reflective coating in segments to avoid formation of eddy currents in the insulation layers.

The individual coils are supported internally as illustrated in Figure 15 with low thermal conductivity members. These supports are designed to take loads in both directions. The high loads per unit length of coil are distributed between supports by a stiff cryostat inner shell.

Equilibrium Field Flux Penetration on the Blanket and Shield

The magnetic field from the EF coils must penetrate the blanket and shield to act on the plasma. The blanket and shield contain much electrically conductive material, particularly stainless steel. Eddy currents in this material would distort the EF and delay its penetration if the blanket and shield were not sufficiently segmented. The blanket and shield design of 16 segments, each made of 3 blocks, imposes very little field distortion and delay of penetration.

Table 6 summarizes the results for calculations of the field induced at the center of the plasma due to the eddy currents in the blanket and shield. Results are expressed as the ratio of the induced field to the applied field and as a phase and time delay.[1]

REFERENCES

1. W. M. Stacey, Jr., et al., "Tokamak Experimental Power Reactor Conceptual Design," ANL/CTR-76-3, Argonne National Laboratory (1976) Chapter IV.
2. R. W. Boom, Private Communication.
3. W. M. Stacey, Jr., et al., "Tokamak Experimental Power Reactor Conceptual Design," ANL/CTR-76-3, Argonne National Laboratory (1976) Chapter III.

TABLE 6. Induced Field in the Plasma Region Due to Eddy Currents in the Segmented or Subdivided Blanket and Shield

Toroidal Segments	Blocks per Segment	Maximum Induced Field B_{in}/B_o	Phase Delay ϕ	Time Delay ϕ
1	1	167%[a]	-	-
8	1	42%[a]	-	-
16	1	9.3%	10.5°	117 ms
32	1	2.3%	2.6°	29 ms
48	1	1.0%	1.1°	12 ms
64	1	0.6%	0.7°	8 ms
16[b]	36	1.5%	1.8°	20 ms

(a) Assumptions of model not valid for these cases.

(b) The 43 blocks per segment in the reference design are represented by 36 blocks per segment in the computational model.